Supporting Information

Bambardekar et al. 10.1073/pnas.1418732112

SI Materials and Methods

Sample Preparation. To mark the cell–cell interface in *Drosophila* embryos, flies double-labeled with E-cadherin::GFP (endogenous promoter) and GAP43::mcherry (squash promotor) were selected. Alternatively, in some cases, Squash::GFP GAP43::mcherry flies were used. Flies were maintained at 25 °C. To obtain embryos, fresh plates were incubated in fly cages for 2–2.5 h. Embryos were collected, dechorionated in bleach solution for 50 s and washed with water. Embryos at the end of cellularization (stage 5 end) were then selected under a dissection microscope and aligned on the edge of the coverslip. Alignment was done with the germ band visible in the imaging plane. For experiments with beads and myosin perturbation, embryos were placed in halocarbon oil and injected using a microinjection setup with either polystyrene beads (1:1,000 stock dilution; Molecular Probes) or ROCK inhibitor (Y-27632; 10 mM; Invitrogen), respectively. Embryos were immersed in water for the light-sheet microscope setup and halocarbon oil for spinning-disk imaging.

Optical Manipulation and Imaging. Optical manipulation of the cell–cell interfaces in individual embryos was done using a custom-built light-sheet microscope (1) coupled with a single-beam gradient trap (1,070-nm wavelength, ytterbium fiber laser; IPG Photonics). A 100× water-immersion lens (1.1 N.A., Nikon) was used for imaging as well as introducing the optical trap in the imaging plane. Imaging was done using 488- and 561-nm excitation lasers. Images were acquired by an EM CCD camera using a dual-view, simultaneous-imaging system. Before every in vivo experiment, we calibrated the relationship between galvanometer voltages and laser trap position using the following procedure: single 500-nm-diameter fluorescent polystyrene beads (fluorescence excitation at 561 nm) were trapped in water and moved slowly by imposing galvanometer voltages (V_1, V_2) of the forms [$V_0\cos(\omega t)$, $V_0\sin(\omega t)$] with $\omega < 0.3$ rad/s. Images were acquired synchronously to the voltage commands, and successive (x, y) positions of the bead were localized by a 2D Gaussian fit. The subpixel localization precision was 25 nm. The measurements were repeated for different voltage amplitudes (corresponding to trap amplitudes in the image plane < 10 μm) providing the relationship between (V_1, V_2) and (x, y), which was subsequently extrapolated linearly and inverted to determine (x, y) as a function of (V_1, V_2) (Matlab script). This information was used to provide laser positions during every interface deflection experiment.

Two kinds of deflections were given to the cell–cell interface: periodic or pull and release. Sinusoidal oscillations of the galvos were performed to produce linear movements of the laser trap, varying time periods from 0.3 to 5 s, amplitudes from 0.3 to 1.1 μm, and laser power from ∼50 to 300 mW (after objective lens). For most experiments, values were kept constant with a time period of 2 s, laser amplitude of 0.5 μm, and laser power at 200 mW. For pull-and-release experiments, the stationary laser trap was switched on at 100 nm—2 μm from the cell–cell interface for between 10 s and 1 min. All experiment recordings were done for galvovoltage as well as the camera images (either at 561- or both 488- and 561-nm excitation).

Quantification of E-cadherin::GFP and Squash::GFP at stage 5 end and stage 7 was done in a Perkin-Elmer spinning-disk microscope using a 100× oil immersion lens.

Quantitative phase imaging uses a transmission light microscope and quadriwave lateral shearing interferometry as described in ref. 2.

Data Analysis. Kymographs of interface deflections were produced from the movies either in Fiji (Multiple Kymograph plugin) or using a custom Matlab script. To extract an actual position of the interface out of the kymograph, a Gaussian fit perpendicular to the interface (along the kymograph line) was performed. At each time step, the peak of the Gaussian fit determines the interface position with subpixel resolution. To determine the localization error, we fixed embryos expressing GapAP43::mcherry and imaged them in the same conditions as in vivo. We then localized cell interfaces over 100 images and found that the SD of localization is 35 nm (10 cell interfaces measured). The interface position together with the optical trap position recorded through the laser voltage were then analyzed in Matlab to measure the response amplitude by maxima detection and averaging. All fits were performed with Matlab: numerical equations were solved repeatedly, exploring the space of parameters starting from random values and using the gradient descent method to minimize error. Statistical analyses were done using the unpaired t test. For the propagation analysis, experimental tissue geometries were extracted using the Tissue Analyzer toolbox by Aigouy et al. (3) and then exported to Matlab to perform the simulations.

The delay between deformations of successive cell–cell contacts in the propagation study was estimated using a custom Matlab script of time-sliding fit. We shifted one signal in time [i.e., we plotted $x(t + \Delta T)$ as a function of the trap position $x_t(t)$]. The time shift ΔT that provides the best linear fit between $x(t + \Delta T)$ and $x_t(t)$ provides an estimate of the time delay between the two signals. The confidence intervals were obtained using the nlparci function of the Matlab statistics toolbox.

Model.

Single junction. The mechanical model for a single junction (fits in Figs. 1*E* and 3*A*) is derived from the constitutive mechanics of the cortex and a force balance equation at the interface. The viscoelastic constitutive equation is given by the so-called standard linear solid model (SLS) and relates the horizontal restoring force f to the deflection x of the interface:

$$\dot{f} + \frac{k_2}{\zeta} f = (k_1 + k_2)\,\dot{x} + \frac{k_1 k_2}{\zeta} x,$$

where k_1 and k_2 are elastic parameters (newtons per meter), ζ is a viscous parameter (meter·pascal·second), and the dot denotes a temporal derivative. At these very low Reynolds numbers, inertia can be neglected, and the balance of forces at the interface then simply reads

$$f = k_t(x_t - x) - C_\eta \dot{x},$$

where k_t and x_t are the stiffness and position of the optical trap, respectively, and C_η is the damping coefficient of the interface in the cytosol. The first term on the right-hand side, thus, corresponds to the force exerted by the optical trap, whereas the second corresponds to the viscous drag in the cytosol and is, therefore, proportional to the velocity $\dot{x}$. This linear system can then be solved for any trap trajectory $x_t(t)$—in particular, for our experimental conditions, a sinusoidal oscillation or a pull-and-release experiment. Moreover, the relaxation timescales associated to this

system can be derived analytically. Combining the constitutive equation and the force balance in the absence of trap yields

$$C_\eta\zeta\,\ddot{x}+\left(C_\eta k_2+\zeta(k_1+k_2)\right)\dot{x}+\;k_1k_2\,x=0.$$

The solution is in the form $x(t)=Ae^{-t/\tau_1}+Be^{-t/\tau_2}$. In the limit $\zeta(k_1+k_2)\gg C_\eta k_2$, which we find is verified from fit values, the two timescales τ_1 and τ_2 simplify into

$$\begin{cases}\tau_1=\dfrac{\zeta(k_1+k_2)}{k_1k_2}\\ \tau_2=\dfrac{C_\eta}{k_1+k_2}\end{cases}.$$

In that limit, one timescale is related to the viscous component of the cortex (ζ), whereas the other is related to the damping coefficient in the cytosol (C_η).

Tissue scale. In the tissue-scale simulations, the epithelium is considered as a network of bonds—the cell contacts—between vertices. Each bond is considered as a viscoelastic segment. The constitutive equation of each segment, similar to the first equation, is

$$\dot{T}+\frac{k_2}{\zeta}T=(k_1+k_2)\,\dot{X}+\frac{k_1k_2}{\zeta}X,$$

where T is the tension, and X is the elongation $X=l-l_0$. The displacement of each vertex is then computed using the force balance equation between the tension at adjacent contact lines $[j=adj(i)]$ and damping in the cytosol ($C_\eta\dot{x}$) (Fig. 3*D*). The force balance at vertex i, thus, reads

$$C_\eta\,\dot{\vec{x}_i}=\sum_{j=adj(i)}\overrightarrow{T_{ij}}\,.$$

This equation provides direct access to vertices displacements through velocities $\dot{\vec{x}_i}$. Notably, the midpoint of the target interface is treated as a two-way vertex in the simulations. Its movement is imposed to mimic the considered experiment. The rest of the vertices move according to the force balance equation; therefore, their movement ultimately results from the deflection movement of the target interface. We use fixed (zero displacement) boundary conditions. The areas are not constrained, because we consider small deformations only. For larger deformations, the model would almost certainly require area or pressure constraints.

1. Chardès C, Mélénec P, Bertrand V, Lenne P-F (2014) Setting up a simple light sheet microscope for in toto imaging of C. elegans development. *J Vis Exp* 87(87):e51342.
2. Bon P, Maucort G, Wattellier B, Monneret S (2009) Quadriwave lateral shearing interferometry for quantitative phase microscopy of living cells. *Opt Express* 17(15): 13080–13094.
3. Aigouy B, et al. (2010) Cell flow reorients the axis of planar polarity in the wing epithelium of Drosophila. *Cell* 142(5):773–786.

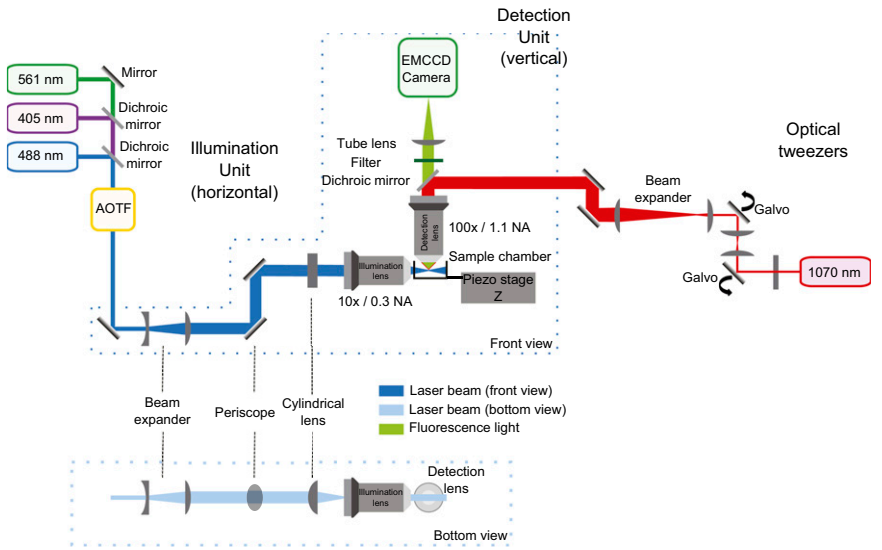

Fig. S1. Optical setup combining light-sheet microscopy and optical tweezers. In the light-sheet illumination unit, the lasers are mixed by the dichroic mirrors and enter the acousto-optical tunable filter (AOTF), which controls the power of each laser independently. Then, the telescope increases the size of the beam by fivefold, and the periscope brings it to the height of the microscope. The cylindrical lens forms the light sheet, which is refocused by the illumination objective. The detection unit is integrated in the upright microscope and mainly composed of the detection lens, the filter, the tube lens, and the EMCCD camera. The sample is positioned at the intersection between the illumination and detection paths. A piezoelectric stage allows vertical (*Z*) displacements of the sample for 3D acquisition. In the optical tweezers unit, a near-IR laser beam (1,070 nm; continuous wave) is deflected by two galvanometric mirrors and expanded by a fivefold telescope. The expanded laser beam is reflected by a hot dichroic mirror and tightly focused by the collection objective of the light-sheet microscope.

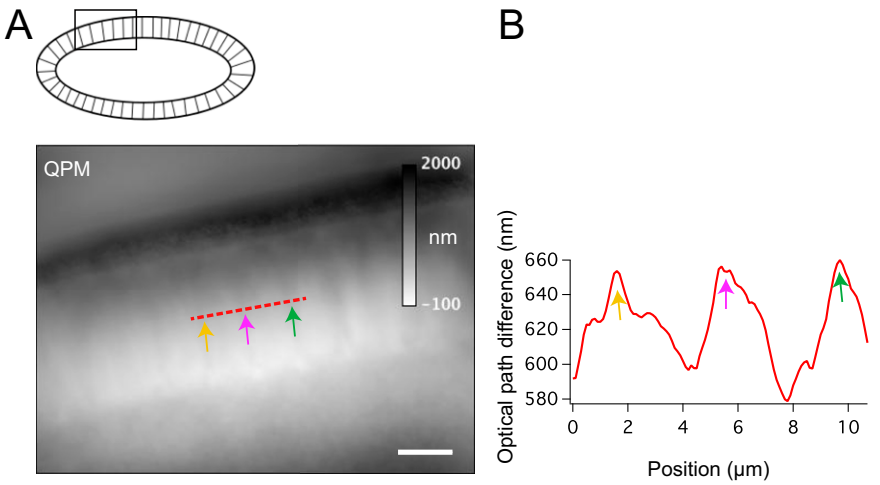

Fig. S2. Phase mismatch at cell interfaces. (*A*) Quantitative phase microscopy (QPM) image obtained from an early *Drosophila* embryo (stage 6). The method uses a transmission light microscope and quadriwave lateral shearing interferometry as described in ref. 1. (*Upper*) The epithelial cells are observed in cross-section (cartoon). (*Lower*) The calibration bar shows the optical path difference in nanometers. (Scale bar: 5 μm.) (*B*) A plot profile along a line (red dotted line in *A*) shows that the optical path difference is larger at cell interfaces than inside the cells. Given that the line defines positions where the geometrical thickness of the embryo is constant, the optical path difference indicates that there is a refraction index increase at cell interfaces. Arrows of different colors mark the positions of three interfaces.

1. Bon P, Maucort G, Wattellier B, Monneret S (2009) Quadriwave lateral shearing interferometry for quantitative phase microscopy of living cells. *Opt Express* 17(15):13080–13094.

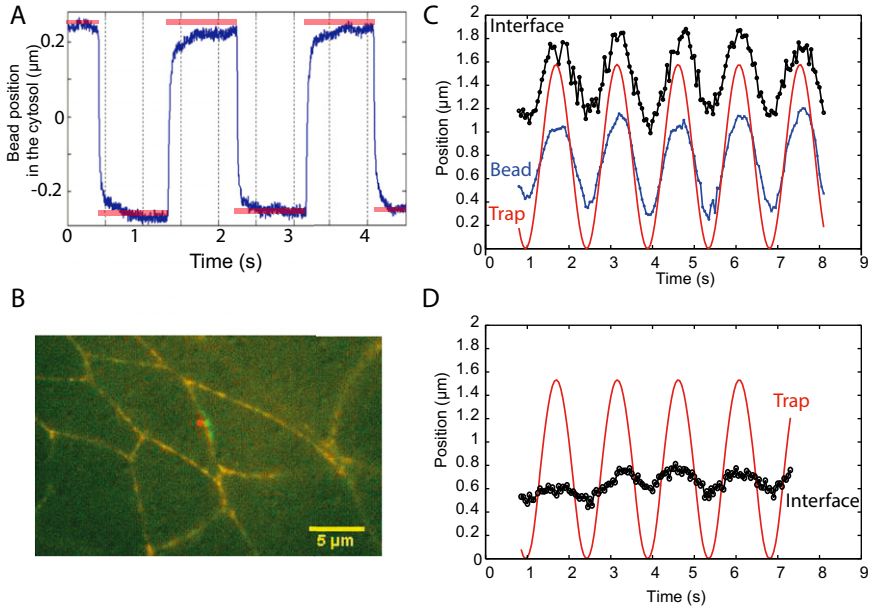

Fig. S3. Deformation induced by optically tweezed beads. (*A*) Position of a 0.46-μm-diameter bead (blue line) in the cytosol moving between two trap positions separated by 0.5 μm (red). From one trap position to another, the bead relaxation is exponential, with a characteristic time given by the ratio of the drag coefficient over the trap stiffness. (*B*) Snapshots of an interface deformation induced by a 0.46-μm-diameter bead moved by the laser trap against the interface. The red and green channels correspond to two different positions of the trap separated by ~0.5 μm. (*C*) Positions of laser trap, bead, and interface in an oscillatory experiment with the bead at 100-mW laser power. (*D*) Positions of the laser trap and the interface in the same conditions as in *C* in the absence of the bead.

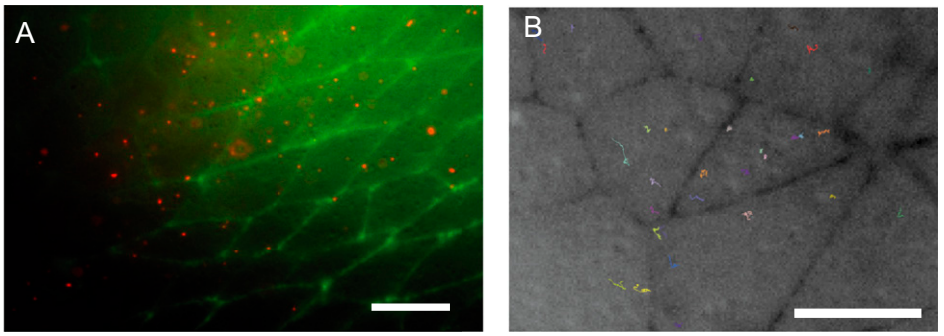

C

Number of embryos	26
Number of beads	4650
Fraction of diffusive beads	0.29
Fraction of superdiffusive beads	0.705
Fraction of subdiffusive beads	0.005

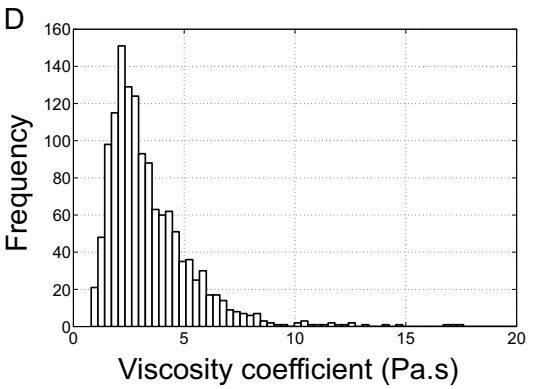

Fig. S4. Viscosity measurements obtained from trajectories of individual beads. (*A*) Image showing 100-nm-diameter beads (red) injected in the embryo. Cell contours are labeled by E-cadherin::GFP. (*B*) Single-particle trajectories superimposed on an image of the cells. (*C*) Fraction of beads exhibiting diffusive, subdiffusive, and superdiffusive behaviors from analysis of the mean square displacement (using criteria as described in ref. 1). Trajectories were acquired at 38 Hz over a time of 13–26 s. Note that the contributions of active fluctuations have been shown to be important below 10 Hz (2), and we cannot fully assert that they do not contribute to bead fluctuations at 38 Hz. Our measurements, thus, provide only an estimate of the cytosol viscosity (effective viscosity). (*D*) Histogram of the viscosity coefficient determined from the analysis of 1,348 particles exhibiting free-like diffusion.

1. Kusumi A, Sako Y, Yamamoto M (1993) Confined lateral diffusion of membrane receptors as studied by single particle tracking (nanovid microscopy). Effects of calcium-induced differentiation in cultured epithelial cells. *Biophys J* 65(5):2021–2040.
2. Mizuno D, Tardin C, Schmidt CF, Mackintosh FC (2007) Nonequilibrium mechanics of active cytoskeletal networks. *Science* 315(5810):370–373.

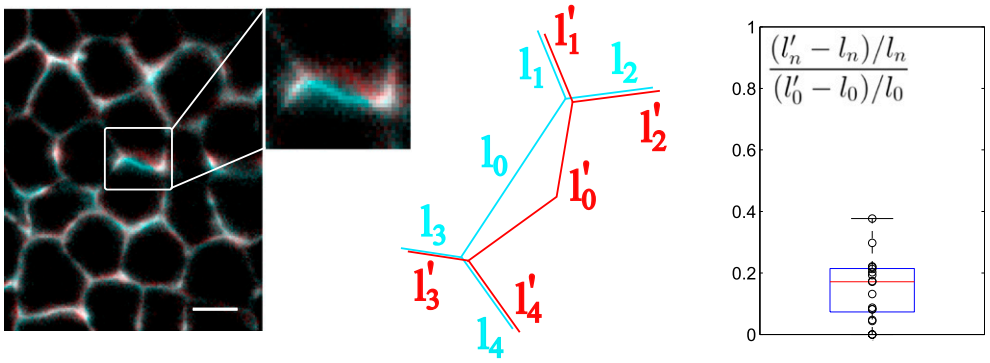

Fig. S5. Elongation of interfaces adjacent to the optically deformed interface; l_0 and l_0' denote the length of the optically tweezed interface before deformation and at maximal deformation, respectively. Elongation of the interface n ($n = 1, 2, 3,$ or 4) adjacent to the interface 0 is given by $l_n' - l_n$. *Left* shows the ratio of $l_n' - l_n$ over $l_0' - l_0$. (*Right*) The red line is the median, the box edges are the lower and upper quartiles, and the whiskers display the total range of measurements. (Scale bar: 5 μm.)

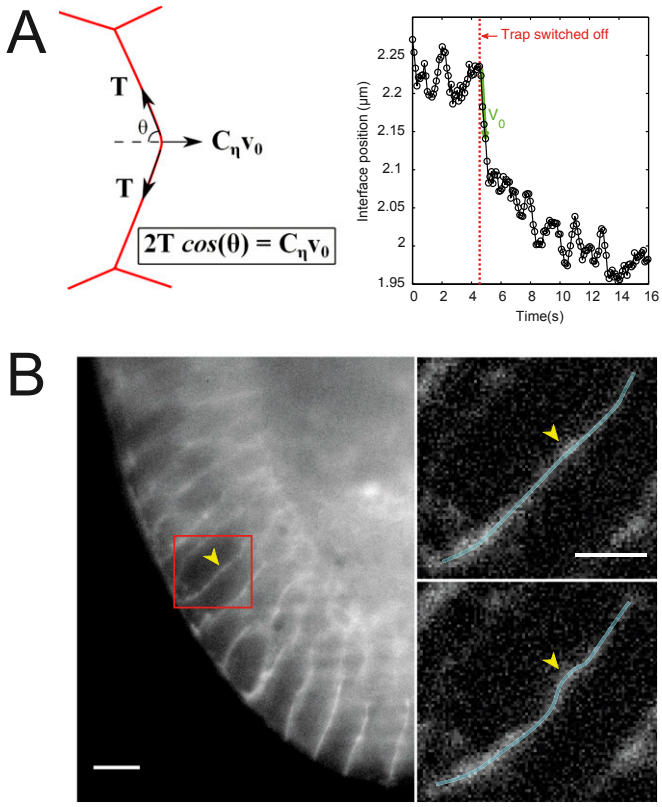

Fig. S6. Relaxation of interfaces after trap release and deformation along the apicobasal axis. (*A*) After trap release, the interface relaxes with an initial velocity, which is dependent on tension and the damping coefficient in the cytosol C_η. (*B*) Deformation of a cell interface in regions of the embryo where the apicobasal axis is in the plane of imaging. (*Left*) The epithelial cells are observed in the cross-section. (*Upper Right*) Interface prior to deflection and (*Left*) deflected interface. (*Lower Right*) The deformation extends over a 4- to 5-μm width along the apicobasal direction. The blue lines are eye guides. (Scale bars: *Left*, 10 μm; *Right*, 5 μm.)

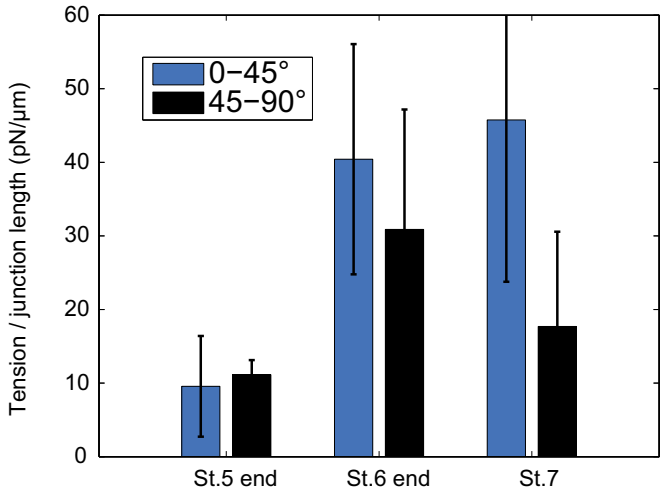

Fig. S7. Tension normalized to junction length along anteroposterior and dorsoventral directions. St., stage.

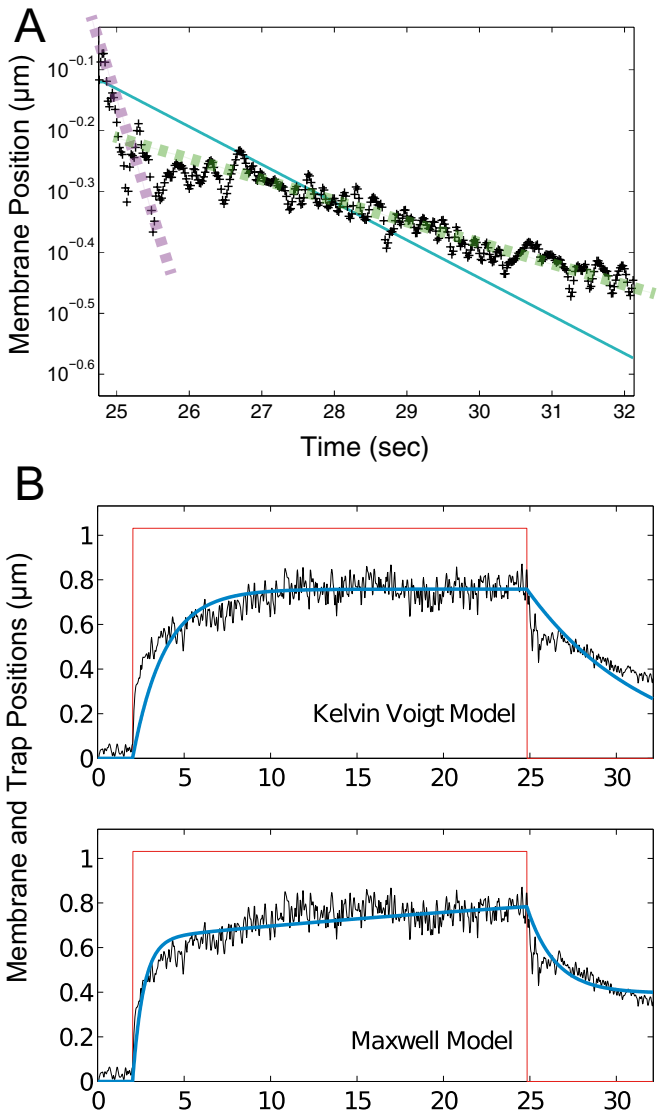

Fig. S8. Pull-and-release experiments and comparison with simple viscoelastic models. (*A*) Relaxation dynamics of the interface in linear log representation. A simple exponential does not fit the data (cyan solid line). The two characteristic times are visible (purple and green dashed lines are eye guides). (*B*) Alternative viscoelastic models for the pull-and-release experiments: (*Upper*) the Kelvin–Voigt model is composed of a spring and a dashpot in parallel, whereas (*Lower*) the Maxwell model is composed of a spring and a dashpot in series. In the presence of external viscosity, both predict exponential relaxation.

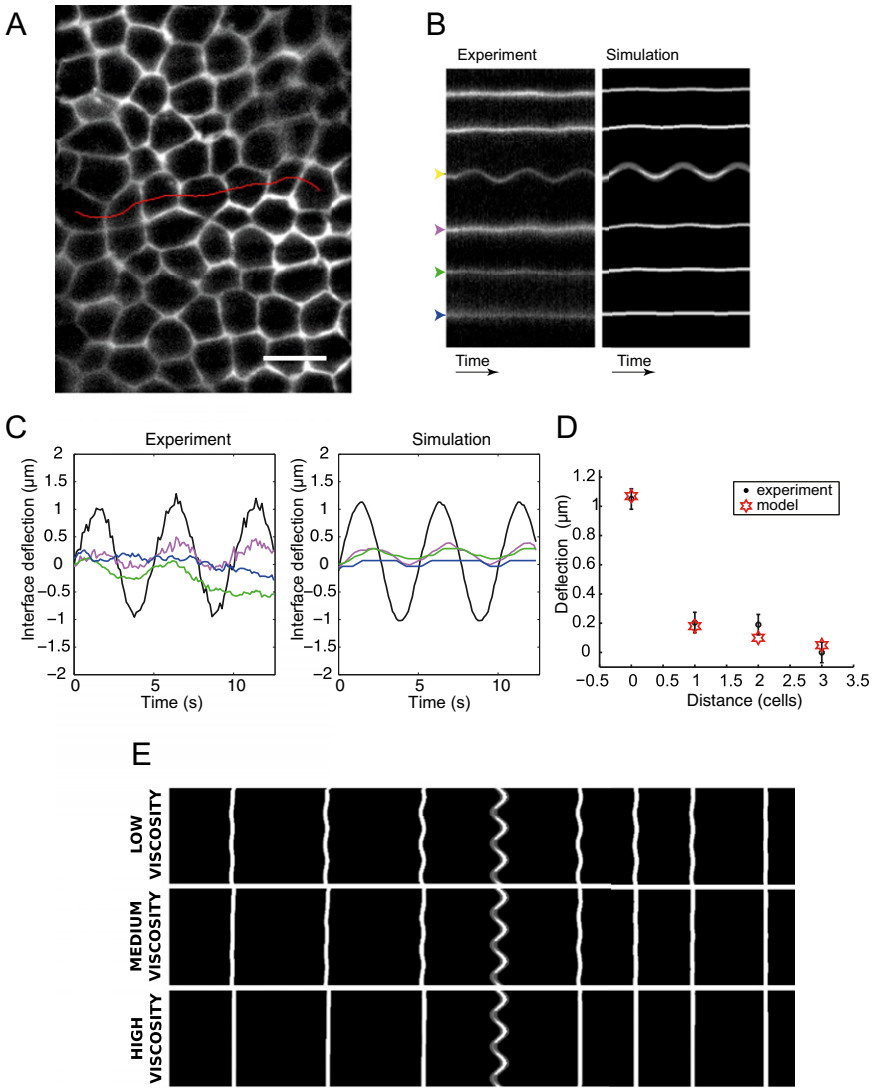

Fig. S9. Mechanical model of the interface and tissue response. (*A*) Deflection perpendicular to the interfaces is tracked over time along lines perpendicular to cell interfaces (red). (Scale bar: 10 μm.) (*B*) Kymograph of interface deflections in the (*Left*) experimental and (*Right*) simulated tissues. (*C*) Deflection of the target (black) and neighbor (at one-, two-, and three-cells distances; magenta, green, and blue, respectively) interfaces in the (*Left*) experimental and (*Right*) simulated tissues. (*D*) Spatial decay of interface deflections over the neighboring cells. Comparison between experiments (●) and simulations (red stars). (*E*) Propagation of deformation for different values of cytosol viscosity (*Top*, viscosity ×20; *Middle*, viscosity ×1; *Bottom*, viscosity ×0.05). A small viscosity results in a more efficient propagation of the deformation, which becomes limited only by the fixed boundary conditions. On the contrary, a high viscosity results in less-efficient propagation.

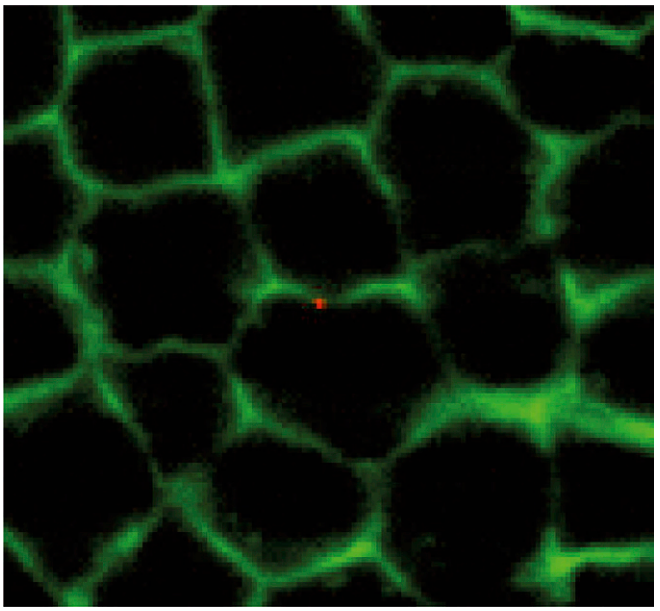

Movie S1. Interface deflection produced by a laser trap (red) after a sinusoidal movement of 0.5-μm amplitude and a 2-s time period.

Movie S1

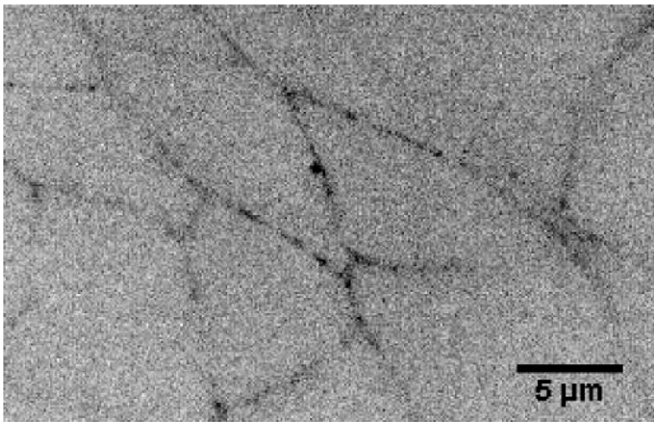

Movie S2. Interface deformation imposed by a laser trap moving a bead against a cell–cell interface.

Movie S2

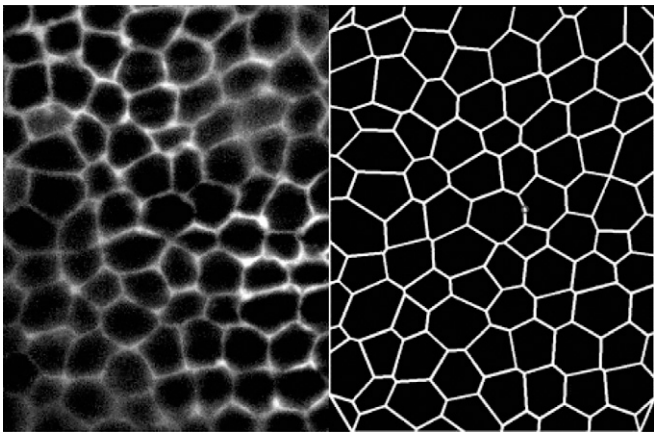

Movie S3. Propagation of local deformation—comparison between in vivo and in silico experiments.

Movie S3